

NONINTERCEPTING BEAM SIZE AND POSITION MONITOR USING ODR FOR X-RAY FELS*

A.H. Lumpkin**, N.S. Sereno, W.J. Berg, D.W. Rule[†], B.X. Yang, and C.-Y. Yao
 Advanced Photon Source, Argonne National Laboratory, Argonne, IL 60439, U.S.A.
[†]Carderock Division, NSWC, West Bethesda, MD 20817 USA.

Abstract

Interest in nonintercepting (NI) beam size and position diagnostics between the undulators of x-ray free-electron lasers (XFELs) is driven by the requirement of beam-emittance matching and beam alignment, as well as by the need to minimize radiation damage to the undulator permanent magnets from scattered beam produced by the insertion of converter screens. For these reasons our investigations on optical diffraction radiation (ODR) as relative beam size and position diagnostics are particularly relevant to XFELs. We report the extensions of our studies at 7-GeV beam energy to aspects of the vertical and horizontal polarization components of the ODR near-field and far-field images. The near-field, vertically polarized data are particularly interesting because the vertical field lines at the metal more directly reflect the actual horizontal beam sizes. Although our experiments to date are with mm-scale beams and impact parameters of 1-2 mm, our analytical model indicates that this technique scales with beam size and has sensitivity at the 20- to 50- μm regime with an impact parameter, $d = 5$ times $\sigma_y = 100 \mu\text{m}$. This is the x-ray FEL intraundulator beam size regime.

INTRODUCTION

The interest in nonintercepting (NI) diagnostics for beam size and position in the undulators of x-ray free-electron lasers (XFELs) for beam match reasons is driven by the need to minimize the radiation damage to the undulator permanent magnets by scattering of beam by inserted converter screens. For such reasons our investigations on optical diffraction radiation (ODR) as NI relative beam size and position diagnostics [1-10] are particularly relevant. We reported initial experiments at FEL05 [11], and now we report the extensions of our studies at 7-GeV beam energy to aspects of the vertical and horizontal polarization components of the ODR near-field and far-field images. It appears that the near-field, vertically polarized data are particularly interesting. For our measurements of the beam size along the horizontal axis with a vertically displaced metal screen, the induced currents from the vertical field lines at the metal more directly reflect the actual beam size as revealed by scans of the upstream quadrupole fields. In addition, in our experimental configuration the vertical polarizer also rejects the strongest component of a weak background of

visible-light optical synchrotron radiation (OSR) generated when the beam transits the horizontal bend dipole magnet that is 5.84-m upstream of the ODR station [12]. This same concept would be applicable to blocking the polarized visible undulator radiation co-propagating with the e-beam in an XFEL.

Although our experiments are with larger beams and impact parameters of 1-2 mm, our analytical model indicates that the technique scales with beam size and has sensitivity at the 20- to 50- μm regime with the impact parameter, $d = 5$ times $\sigma_y = 100 \mu\text{m}$. The beam size is similar to the 30- μm beam size in the XFEL intraundulator location. In addition, a direct comparison of the horizontal position readings of the nearby rf beam position monitor (BPM) and the ODR image centroid values during the scan of the upstream dipole current showed good agreement. The ODR data were also found to be very similar to an OTR image value during a similar dipole current scan. Our experimental results and some modeling results will be presented.

EXPERIMENTAL BACKGROUND

The Advanced Photon Source (APS) facility includes an injector complex with an rf thermionic cathode gun, an S-band linear accelerator, a particle accumulator ring (PAR) that damps the linac beam at 325 MeV, a booster injector synchrotron that ramps the energy from 0.325 GeV to 7 GeV in 220 ms, and the 7-GeV storage ring. At the exit of the booster, a dipole magnet allows direction of the beam to an alternate booster extraction beamline (BTX) that ends with a beam dump. This spur line has been used to develop our optical transition radiation (OTR) and our ODR diagnostics. The setup includes the upstream corrector magnets, two quadrupoles, and a dipole; and then, 5.8-m downstream the rf BPM (horizontal), the OTR/ODR imaging station, a localized beam-loss monitor based on a Cherenkov radiation detector, a Chromox beam-profiling screen, and the beam dump, as schematically shown in Fig. 1. An additional feature of the remote control of one strategic lens changes the optics from near-field to far-field imaging.

The ODR converter is a polished Al blade/mirror that is 1.5-mm thick, 30-mm wide, 30-mm tall, and it is mounted with its surface normal at 45° to the beam direction on a vertical stepper assembly. Its horizontal edge can be vertically positioned with an overall accuracy of $\pm 10 \mu\text{m}$ over a span of 27.5 mm. The alignment of the optics with converter surface angle was done with an alignment laser placed on the surveyed beamline axis during an access

*Work supported by the U.S. Department of Energy, Office of Science, Office of Basic Energy Sciences, under Contract No. W-31-109-ENG-38.

**lumpkin@aps.anl.gov

period as described previously [12]. The near-field magnification resulted in calibration factors of 60- μm per pixel in x and 45- μm per pixel in y. Two 6-position filter wheels were used to select neutral density (ND) filters, bandpass filters, or two polarizers, which are oriented at 90 degrees to each other. The images are detected with a standard SONY charge-coupled device (CCD) camera, and the video is digitized with a MaxVideo MV200 digitizer interfaced to the Experimental Physics and Industrial Control Systems (EPICS) software architecture. The online image processing allows the selection of a region of interest, formation of the projected x and y profiles, and both a Gaussian fit to the profile and a numerical evaluation of the FWHM of the profile. The rms size is then the sigma of the Gaussian result or the estimated value found by dividing the numerically calculated FWHM by 2.35.

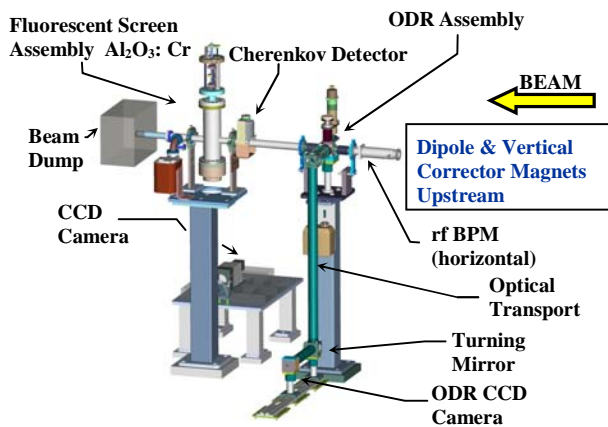


Figure 1: A Pro-E drawing of the OTR/ODR imaging station showing the rf BPM, the cube and stepper drive, the optical transport, the Cherenkov detector local loss monitor, and the Chromox profile monitor.

EXPERIMENTAL AND ANALYTICAL RESULTS

As mentioned in the previous section, the ODR profile results are referenced to complementary OTR profile results, and the image centroids are compared to the nearby, upstream rf BPM. The SDDS tools are used for the tracking of the process variables [13, 14].

The potential to monitor relative beam size has been discussed in our earlier papers [11, 12, 15]. However, in this case we now have the results of vertically polarized data. The OTR image profiles were first obtained by inserting the Al metal screen during a scan of the upstream AQ2 quadrupole field. This quadrupole strongly affects the horizontal beam size at our OTR/ODR station. Unfortunately, this is at a dispersive point in the lattice so we do not get emittance data cleanly from the quadrupole field scan. However, we do obtain a test of ODR as a relative beam size monitor. As seen in Fig. 2, the unpolarized, OTR-measured horizontal beam size varies from 2300 μm down to about 1300 μm . Results of both algorithms are shown, and they are seen to be in very good agreement because the beam shape is basically

Gaussian when extracted from the 7-GeV booster synchrotron. Next, in Fig. 3, we show the observed vertically polarized ODR image profiles with an impact parameter of 1.25 mm during a similar quadrupole field scan. The vertically polarized ODR horizontal image profiles track the beam size changes as seen qualitatively by the shape of the curve with AQ2 current. A direct comparison of the OTR and ODR is seen in the Fig. 4 combined plot of their fitted rms values. The ODR profiles are about 10% to 25% larger than the corresponding OTR profiles from the largest beam size to the smallest, respectively. The ratio of ODR/OTR for the size scan is next plotted in Fig. 5 to act as a lookup table for the beam-size monitor. As can be seen, at the minimum size of 1300 μm for the OTR, the ODR fit value is only 25% larger. This is much better than our factor of two results with unpolarized ODR observed on the same shift for this minimum beam focus and also reported at BIW06 [12]. The vertical polarization component would appear to be more reliable and direct in monitoring the actual beam size to better than 10% one has the ratio table or plot for these conditions.

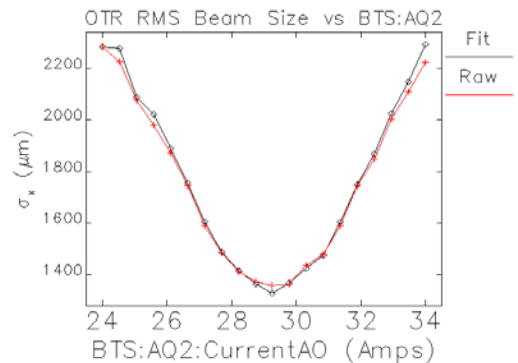


Figure 2: A plot of the OTR rms horizontal profile sizes for the upstream AQ2 quadrupole field scan. Both a Gaussian fit and a simple peak intensity to FWHM algorithm were used, which are in good agreement.

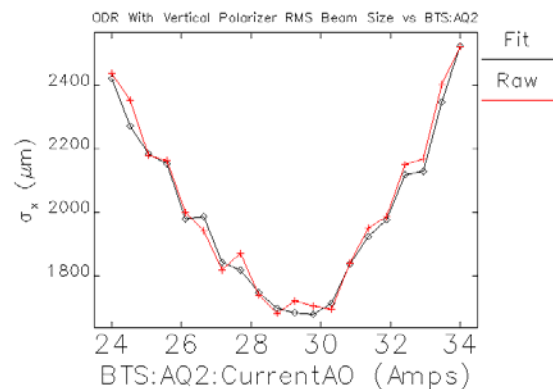


Figure 3: A plot of the vertically polarized ODR rms horizontal profile sizes for the upstream AQ2 quadrupole field scan. Both a Gaussian fit and a simple peak intensity to FWHM algorithm were used to measure image sizes, which are in good agreement.

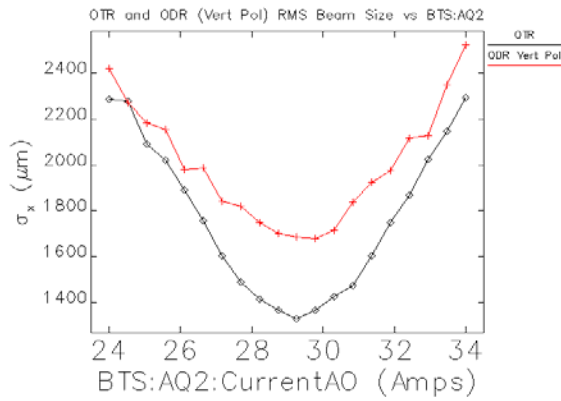


Figure 4: A direct comparison of the ODR (plus) and OTR (diamonds) Gaussian-fit horizontal profile size s during the quadrupole field scan. The vertically polarized ODR tracks the beam-size changes.

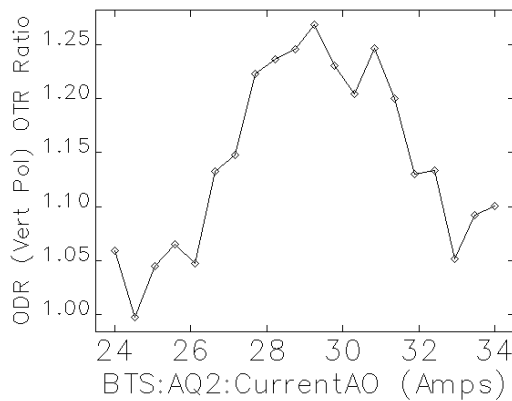


Figure 5: The ratio of ODR/OTR horizontal image sizes for different beam sizes during the AQ2 quadrupole scan. This ratio is noticeably smaller than for unpolarized data reported earlier.

In Fig. 6, we show the analytical results from our model described previously [11] for a beam size change of $\pm 20\%$ around the nominal $\sigma_x = 1300\text{-}\mu\text{m}$ value and the corresponding ODR image profile changes at the $1/e$ points in intensity. First, it is clear there is sensitivity to the beam-size changes that should be detectable in the camera images. Second, the HWHM values indicate an ODR profile of about 1.2 times the actual beam size as seen in the polarized data comparisons. These were done with a fixed $\sigma_y = 200\text{ }\mu\text{m}$. Initial vertical polarization effects have also been calculated, but further work is needed. The calculated ODR x width using the vertical polarization component was 20 to 50% narrower than that calculated using the horizontal component for $d = 1000$ and $2000\text{ }\mu\text{m}$, respectively.

We also have calculated the sensitivity of ODR profiles to smaller beam sizes. In this case, we held the y size constant at $20\text{ }\mu\text{m}$ and varied the x -size from 20 to $50\text{ }\mu\text{m}$ using an impact parameter of $100\text{ }\mu\text{m}$ and beam energy of 7 GeV . In Fig. 7 it is clear that approximately a 25% increase in the ODR horizontal profile half width is

calculated for the $50\text{-}\mu\text{m}$ beam size. Image processing should easily detect this change and use of polarization would improve the sensitivity. This should be a good match to monitoring beams of $30\text{-}\mu\text{m}$ size in the XFELs, subject to signal levels.

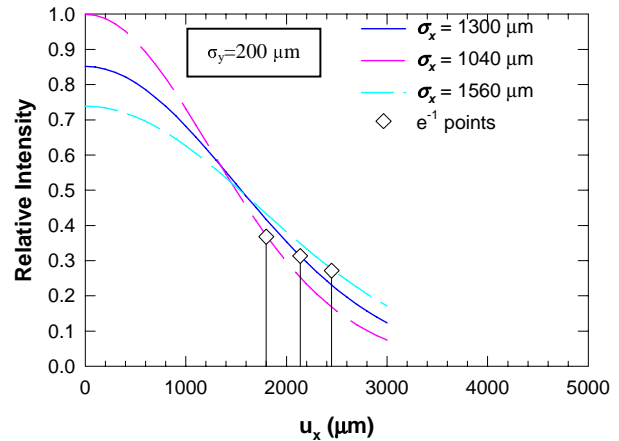


Figure 6: Analytical model results for the effects on the unpolarized ODR horizontal profiles for a variation of the beam size by $\pm 20\%$ around the $1300\text{-}\mu\text{m}$ value with $d = 1000\text{ }\mu\text{m}$.

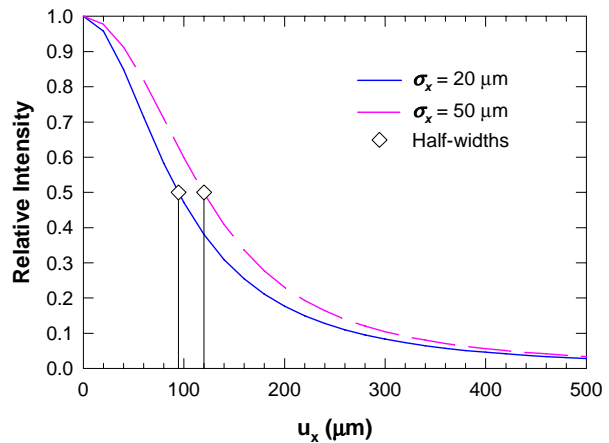


Figure 7: Analytical results for the change in unpolarized, horizontal ODR profiles for a change in beam size from 20 to $50\text{ }\mu\text{m}$ while holding the y value constant at $20\text{ }\mu\text{m}$. The impact parameter is $100\text{ }\mu\text{m}$ for the 7-GeV beam. This is relevant to XFEL beam-size monitoring.

In addition, we repeated our relative beam position measurements first done with unpolarized ODR and compared to the rf BPM and OTR values [11]. In this case, we again used vertically polarized ODR with an impact parameter, $d = 1.25\text{ mm}$ and a vertical size σ_y of $200\text{ }\mu\text{m}$ or less. The plot in Fig. 8 actually compares the centroid values from both OTR and ODR to the horizontal BPM readings. The OTR and ODR data overlap each other almost completely. This was done with the beam size $\sigma_x = 1300\text{ }\mu\text{m}$, the AQ2 quadrupole field set for the beam size minimum. Again, we believe the vertically polarized ODR component benefits the measurement sensitivity in the horizontal axis. Sensitivity at the 50-

100- μm relative position level is attained. As in the case of beam size monitoring, for the much smaller beam and impact parameter in the XFEL case, we would expect much better position sensitivity (sub-10 μm) subject to signal level. Correspondingly, a vertical, single edge of a metal screen or aperture can be employed to obtain information on vertical position and beam size.

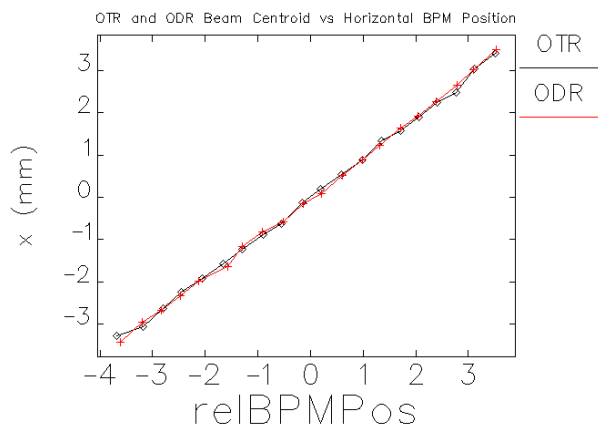


Figure 8: A plot of the OTR and ODR centroid value changes versus the nearby rf BPM values in mm during a scan of the upstream dipole current supply (and magnet fields). Horizontal position information can be reliably obtained from the vertically polarized ODR image centroids.

SUMMARY

In summary, we have extended our NI diagnostics techniques by evaluating the vertical and horizontal polarization components of near-field ODR images. As expected, the induced currents from the vertical field lines more directly represent the horizontal beam size in our configuration. Our results indicate that the tracking of relative beam size and position can be scaled down to address the potential needs of x-ray FELs. Complementary information on beam trajectory angle and beam divergence is being explored as well for higher average current beams.

ACKNOWLEDGMENTS

The authors acknowledge the support of Brian Rusthoven, Al Barcikowski, and Mike Bracken in the Mechanical Engineering Group, Joe Gagliano and Wayne Michalek in the Vacuum Group, Chuck Gold of the Diagnostics Group, and Bill Jansma and Horst Friedsam in the Survey Group for installation and resurvey, respectively, of the station in December 2005 and January 2006. The laser alignment proved to be a critical contribution to the new optics setup and the rotated BPM addressed the horizontal plane request.

REFERENCES

1. A.P. Kazantsev and G.I. Surdutovich, *Sov. Phys. Sokl.* **7**, 990 (1963).
2. M.L. Ter-Mikaelian, *High Energy Electromagnetic Processes in Condensed Media* (Wiley/Interscience, New York, 1972).
3. M. Castellano, *Nucl. Instrum. Methods A* **394**, 275 (1997).
4. Y. Shibata et al., *Phys. Rev. E* **52**, 678 (1995).
5. A.P. Potylitsyn, *Nucl. Instrum. Methods B* **145**, 169 (1998).
6. R.B. Fiorito, D.W. Rule, and W.D. Kimura, *AIP Conf. Proc.* **472**, 725 (1999); W.D. Kimura, R.B. Fiorito, and D.W. Rule, *Proc. of the 1999 Particle Accelerator Conference*, 487 (1999).
7. D.W. Rule, R.B. Fiorito, and W.D. Kimura, *AIP Conf. Proc.* **390**, 510 (1997).
8. R.B. Fiorito and D.W. Rule, *Nucl. Instrum. Methods B* **173**, 67 (2001).
9. T. Muto et al., *Phys. Rev. Lett.* **90**(10) 104801-1 (2003).
10. P. Karataev et al., *Phys. Rev. Lett.* **93**, 244802 (2004).
11. A.H. Lumpkin et al., "Nonintercepting Electron Beam Diagnostics Based on Optical Diffraction Radiation for X-ray FELs," *Proceedings of the International FEL05 Conference, Stanford, CA, Aug. 21-26, 2005, JACoW/eConfC0508213*, p. 604.
12. A.H. Lumpkin et al., "Developments in OTR/ODR Imaging Techniques for 7-GeV Electron Beams at APS," submitted to *Proceedings of BIW06, Batavia, Illinois, May 1-4, 2006*.
13. L. Emery, M. Borland, H. Shang, R. Soliday, "User's Guide for SDDS-Compliant EPICS Toolkit Version 1.5," *Advanced Photon Source, March 9, 2005*.
14. H. Shang, *Proc. of PAC2003*, 3470 (2003).
15. A.H. Lumpkin et al., "Near-Field Imaging of Optical Diffraction Radiation Generated by a 7-GeV Electron Beam," submitted to *Phys. Rev.*